

$\Xi(1530)$ production in K^-p scattering process

Quan-Yun Guo^{1,*}, Jing Liu^{2,†}, Peiwen Wu^{1,‡} and Dian-Yong Chen^{1,3,§}

¹ School of Physics, Southeast University, Nanjing 210094, People's Republic of China

² School of Physics and Mechanical Electrical and Engineering,
Hubei University of Education, Wuhan 430205, China and

³ Lanzhou Center for Theoretical Physics, Lanzhou University, Lanzhou 730000, China

(Dated: July 4, 2025)

In the present work, we investigate the production of $\Xi(1530)$ in the $K^-p \rightarrow K^+\Xi(1530)^-$ and $K^-p \rightarrow K^0\Xi(1530)^0$ processes by utilizing an effective Lagrangian approach. In order to fit the cross sections for both processes, we include nine Λ/Σ hyperons and their resonances in the s - and u -channel processes. Due to the inconsistency of the measured cross sections for $K^-p \rightarrow K^+\Xi(1530)^-$ in the range $\sqrt{s} = [2.087, 2.168]$ GeV, we perform the fitting with all the experimental data having the same weight (model A) and different weight (model B) in the present work. Based on a comparative analysis of the fit results in two models, we conclude that Model A demonstrates a better global agreement with the experimental data than Model B. In addition to the cross sections, the individual contributions from different intermediate states to the cross sections are also estimated. Our results indicate that the cross section resulted from $\Sigma(1193)$ intermediate process is predominant. Moreover, the different cross sections are predicted for both the charged and neutral processes with several typical center-of-mass energies, which could be tested by further experimental measurements at J-PARC in the future.

I. INTRODUCTION

Ξ hyperons, composed of one up or down quark and two strange quarks, are particularly interesting members of the baryon family because they provide insights into the dynamics of the strong force in environments with high strange quark content. Due to this characteristic, the production of Ξ hyperons is challenging, and experimental observations are limited compared to Λ and Σ hyperons, which contain only one strange quark. A review of the Particle Data Group (PDG) reveals that only the ground S -wave states, $\Xi(1315)^{0,-}$ with $J^P = 1/2^+$ and $\Xi(1530)$ with $J^P = 3/2^+$, are well-established with four-star ratings [1]. Additionally, there are four Ξ resonances with three-star ratings: $\Xi(1690)$, $\Xi(1820)$, $\Xi(1950)$, and $\Xi(2030)$. Of these, the J^P quantum numbers of $\Xi(1820)$ have been determined to be $3/2^-$, and the spin of $\Xi(2030)$ has been measured to be $5/2$. The remaining five Ξ resonances, $\Xi(1620)$, $\Xi(2120)$, $\Xi(2250)$, $\Xi(2370)$, and $\Xi(2500)$, are only rated as two- or one-star in the PDG [1], indicating that their existence is only considered to be fairly or even poorly established.

Experimental knowledge of the Ξ hyperon spectrum is severely limited. As highlighted by the Particle Data Group review, a significant portion of the current data on Ξ hyperons derives from low-statistics experiments conducted in the 1960s-1980s with K^- beams, and in the 1980s and 1990s with hyperon (Σ^- , Ξ^-) beams [1]. Despite these limitations, advancements have emerged from collider experiments. Several excited Ξ hyperons have been identified in the decay products of charmed baryons. Notably, the Belle Collaboration detected the $\Xi(1690)$ hyperon in the Σ^+K^- invariant mass from

$\Lambda_c^+ \rightarrow \Sigma^+K^-K^+$ decays [2], subsequently confirmed by BaBar in the $\Xi^-\pi^+$ channel from $\Lambda_c^+ \rightarrow \Xi^-\pi^+K^+$ [3]. Belle Collaboration also made the initial observation of $\Xi(1620)^0$ decaying to $\Xi^-\pi^+$ through $\Xi_c^+ \rightarrow \Xi^-\pi^+\pi^+$ decays [4]. Furthermore, the CLAS Collaboration has contributed through the measurement of $\Xi(1321)^-$ hyperon photoproduction via the reactions $\gamma p \rightarrow K^+K^+\Xi^-$ and $\gamma p \rightarrow K^+K^+\pi^-\Xi^0$ [5, 6], enabling them to obtain a substantial sample of $\Xi(1321)^-$. Using a subsequent, high-statistics dataset for the reactions $\gamma p \rightarrow K^+K^+(X)$ and $\gamma p \rightarrow K^+K^+\pi^-(X)$ [7], the CLAS collaboration measured a mass splitting for the ground state (Ξ^- , Ξ^0) doublet, which is (5.4 ± 1.8) MeV [7].

On the theoretical side, comprehensive investigations of the Ξ spectrum have been undertaken using various approaches. For instance, the spectrum and decay properties of Ξ hyperons have been estimated within the constituent quark model, including relativistic [8] and non-relativistic versions with harmonic confinement potentials [9–11] or linear plus Coulomb potentials [12]. Furthermore, Ref. [13] explores the spectrum and decay properties of Ξ hyperons using a string-like model, where radial excitations are interpreted as rotations and vibrations of the strings. Masses of negative-parity Ξ hyperons have also been analyzed in large N_c QCD, considering corrections to order $1/N_c$ and first-order SU(3) symmetry breaking [14]. Additionally, the mass spectrum and magnetic moments of Ξ baryon resonances have been investigated within the bound-state framework of the Skyrme model [15].

From the perspective of the productions of Ξ states, the two-body process $K^-N \rightarrow K^+\Xi$ is the only feasible binary reaction, while other projectiles such as photons, pions, protons, invariably lead to multi-body final states involving three or more particles. The experimental investigations of K^-p scattering began nearly sixty years ago. For example, in Ref. [16] the productions of Ξ^- and Ξ^0 hyperons in K^-p interactions between 1.05 and 1.7 GeV were measured, and the cross sections were reported to be about $150 \mu\text{b}$ for Ξ^-K^+ production and $100 \mu\text{b}$ for Ξ^0K^0 and $\Xi\pi K$ productions, in addition to which

*Electronic address: guoquanyun@seu.edu.cn

†Electronic address: liujing@hue.edu.cn

‡Electronic address: pwwu@seu.edu.cn

§Electronic address: chendy@seu.edu.cn

the production of $\Xi^*(1530)$ near threshold was also observed. Meanwhile, the Ξ -hyperon production in the K^-p interaction at 2.24 GeV [17] and 3.5 GeV [18] were measured. After that the production cross sections and differential cross sections of $\Xi(1314)$ and $\Xi(1530)$ in the K^-p scattering were further reported at different incident kaon beam momenta till to 1977 [19–27]. It is worth noting that the High-Energy Reactions Analysis Group in CERN [28] presented a lot of cross-sectional experimental data about $\Xi(1314)^{0,-}$ and $\Xi(1530)^{0,-}$ in the Kp scattering processes in 1979, which provides experimental conditions for our study on the production of $\Xi(1530)$.

In the early theoretical researches, there were only a few work progresses on the production of Ξ hyperons due to the limitation of experimental data. In Ref. [29], the authors explained the backward production features of the reaction $K^-p \rightarrow \Xi^-K^+$ by using the two-meson-exchange peripheral model, in which the cross sections and the angular distributions for the reaction $K^-p \rightarrow \Xi^-K^+$ could be well described by using the two-meson-exchange box diagrams. Within the model based on Regge theory, duality and SU(3) symmetry combined with the known data, the authors in Ref. [30] investigated the reaction $\bar{K}N \rightarrow \Xi K$ at high energy.

In 2011, the production of $\Xi(1314)$ in the K^-N scattering process was investigated in Ref. [31], where the cross sections and differential cross sections for the $K^-N \rightarrow K\Xi(1314)$ were fitted within the Phenomenological model. By utilizing the effective Lagrangian approach, the s - and u -channels exchange by Λ , Σ , and their resonances were taken into considerations, and they found that the cross sections and differential cross section could be well described. Similarly, in Ref. [32], the authors also investigated the process $\bar{K}N \rightarrow \Xi K$ in the effective Lagrangian method. It is worth noting that in addition to the contributions of s - and u -channels, a contact diagram was also included, and their estimations showed that the dominant contribution came from the contact diagram, while the s - and u -channels contributions were only about 20% of that of the contact term.

Besides the production of $\Xi(1314)$ in the K^-p scattering process, we also notice that there are some data related to cross sections for $K^-p \rightarrow K^+\Xi(1530)^-$ and $K^-p \rightarrow K^0\Xi(1530)^0$ in Ref. [16, 22, 27, 28]. In addition, the extension project has been proposed in the J-PARC hadron experimental facility, where the high energy kaon beam with high quality can be available. With the kaon beam, the production of Ξ -hyperon, including $\Xi(1530)$, will be possible. Thus, we propose to investigate the processes $K^-p \rightarrow K^+\Xi(1530)^-$ and $K^-p \rightarrow K^0\Xi(1530)^0$ simultaneously in the present work. The model parameters for both the charged and neutral processes could be determined by fitting within the Phenomenological model, and then the cross sections could be estimated with these parameters. In addition, the predicted differential cross sections for $K^-p \rightarrow K\Xi(1530)$ could be further tested by the experimental measurements at J-PARC in the future.

This work is organized as follows. After the Introduction, the effective approach employed to investigate the processes $K^-p \rightarrow K\Xi(1530)$ are presented. In Section III, the numerical results and related discussions of the cross sections and the differential cross sections for the relevant processes are

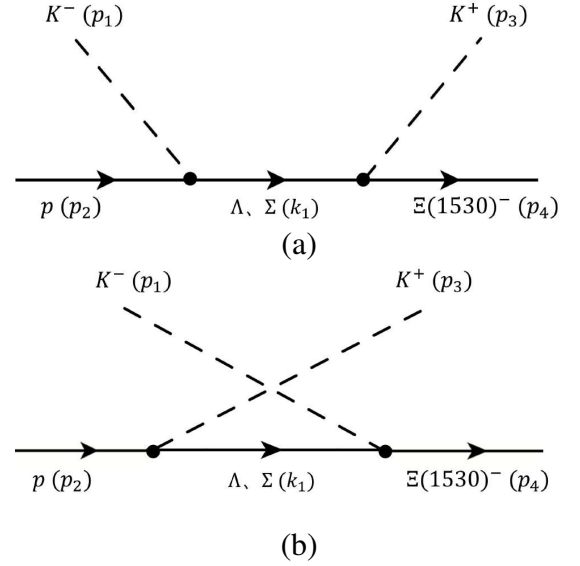


FIG. 1: Diagrams contributing to the process of $K^-p \rightarrow K^+\Xi(1530)^-$, in which (a) and (b) correspond to the s - and u -channel contributions, respectively.

presented. The last section is devoted to a summary.

II. $\Xi(1530)$ PRODUCTION IN THE Kp SCATTERING PROCESS

In the present work, we employ the effective Lagrangian approach to describe the production of $\Xi(1530)$ in the K^-p scattering process. The diagrams contributing to $K^-p \rightarrow K^+\Xi(1530)^-$ are presented in Fig. 1, where the Λ/Σ hyperons and their resonances could serve as intermediate states. In the present calculations, we refer Y_{JP} to the Λ/Σ hyperon and their resonances with spin J and parity P , and the effective Lagrangians for $pY_{1/2^\pm}K$ read [32],

$$\mathcal{L}_{pY_{1/2^\pm}K} = (\mp i)f_{pY_{1/2^\pm}K}\bar{p}\left\{\begin{matrix} \gamma_5 \\ 1 \end{matrix}\right\}Y_{1/2^\pm}K + H.c., \quad (1)$$

with the upper and lower symbols in the curly bracket to be the positive and negative parity of Y hyperon, respectively. For the $pY_{3/2^\pm}K$ coupling, the effective Lagrangians are [32],

$$\mathcal{L}_{pY_{3/2^\pm}K} = \frac{f_{pY_{3/2^\pm}K}}{m_\pi}\bar{p}\left\{\begin{matrix} 1 \\ \gamma_5 \end{matrix}\right\}Y_{3/2^\pm}^\mu\partial_\mu K + H.c. \quad (2)$$

In addition, for the hyperon with $J^P = 5/2^\pm$ and $J^P = 7/2^\pm$, the relevant effective Lagrangians read [32],

$$\begin{aligned} \mathcal{L}_{pY_{5/2^\pm}K} &= (-i)\frac{f_{pY_{5/2^\pm}K}}{m_\pi^2}\bar{p}\left\{\begin{matrix} \gamma_5 \\ 1 \end{matrix}\right\}Y_{5/2^\pm}^{\mu\nu}\partial_\mu\partial_\nu K + H.c., \\ \mathcal{L}_{pY_{7/2^\pm}K} &= (-1)\frac{f_{pY_{7/2^\pm}K}}{m_\pi^3}\bar{p}\left\{\begin{matrix} 1 \\ \gamma_5 \end{matrix}\right\}Y_{7/2^\pm}^{\mu\nu\rho}\partial_\mu\partial_\nu\partial_\rho K + H.c., \end{aligned} \quad (3)$$

respectively. In addition, for $\Xi(1530)Y_{J^P}K$ coupling, the relevant effective Lagrangians can be,

$$\begin{aligned}\mathcal{L}_{\Xi'Y_{1/2^\pm}K} &= \frac{f_{\Xi'Y_{1/2^\pm}K}}{m_\pi}\bar{\Xi}'^\mu\left\{\frac{1}{\gamma_5}\right\}Y_{1/2^\pm}\partial_\mu K + H.c., \\ \mathcal{L}_{\Xi'Y_{3/2^\pm}K} &= (\mp i)f_{\Xi'Y_{3/2^\pm}K}\bar{\Xi}'^\mu\left\{\frac{\gamma_5}{1}\right\}Y_{3/2^\pm}^\mu K + H.c., \\ \mathcal{L}_{\Xi'Y_{5/2^\pm}K} &= \frac{f_{\Xi'Y_{5/2^\pm}K}}{m_\pi}\bar{\Xi}'^\mu\left\{\frac{1}{\gamma_5}\right\}Y_{5/2^\pm}^{\mu\nu}\partial_\nu K + H.c., \\ \mathcal{L}_{\Xi'Y_{7/2^\pm}K} &= (-i)\frac{f_{\Xi'Y_{7/2^\pm}K}}{m_{\pi^2}}\bar{\Xi}'^\mu\left\{\frac{\gamma_5}{1}\right\}Y_{7/2^\pm}^{\mu\nu\rho}\partial_\nu\partial_\rho K + H.c.,\end{aligned}\quad (4)$$

respectively. Hereafter the Ξ' refers to $\Xi(1530)$. In addition, the Λ/Σ hyperon and their resonances [1] involved in the present estimations are collected in Table I. With the above effective Lagrangians, one can obtain the amplitudes of the $K^-p \rightarrow K^+\Xi(1530)^-$ process, which are,

$$\begin{aligned}\mathcal{M}_{Y_{1/2^+}}^s &= \bar{u}_\mu(p_4, m_4)\left[\frac{f_{\Xi'Y_{1/2^+}K}}{m_\pi}(ip_3^\mu)\right]\left[S^{1/2}(k_1, m_Y, \Gamma_Y)\right]\left[-if_{pY_{1/2^+}K}\gamma_5\right]u(p_2, m_2)F(q_i^2, \Lambda_a^2)F(q_f^2, \Lambda_a^2), \\ \mathcal{M}_{Y_{1/2^+}}^u &= \bar{u}_\mu(p_4, m_4)\left[\frac{f_{\Xi'Y_{1/2^+}K}}{m_\pi}(-ip_1^\mu)\right]\left[S^{1/2}(k_1, m_Y, \Gamma_Y)\right]\left[-if_{pY_{1/2^+}K}\gamma_5\right]u(p_2, m_2)F(q_i^2, \Lambda_a^2)F(q_f^2, \Lambda_a^2), \\ \mathcal{M}_{Y_{1/2^-}}^s &= \bar{u}_\mu(p_4, m_4)\left[\frac{f_{\Xi'Y_{1/2^-}K}}{m_\pi}\gamma_5(ip_3^\mu)\right]\left[S^{1/2}(k_1, m_Y, \Gamma_Y)\right]\left[if_{pY_{1/2^-}K}\right]u(p_2, m_2)F(q_i^2, \Lambda_a^2)F(q_f^2, \Lambda_a^2), \\ \mathcal{M}_{Y_{1/2^-}}^u &= \bar{u}_\mu(p_4, m_4)\left[\frac{f_{\Xi'Y_{1/2^-}K}}{m_\pi}\gamma_5(-ip_1^\mu)\right]\left[S^{1/2}(k_1, m_Y, \Gamma_Y)\right]\left[if_{pY_{1/2^-}K}\right]u(p_2, m_2)F(q_i^2, \Lambda_a^2)F(q_f^2, \Lambda_a^2), \\ \mathcal{M}_{Y_{3/2^+}}^s &= \bar{u}_\mu(p_4, m_4)\left[-if_{\Xi'Y_{3/2^+}K}\gamma_5\right]\left[S_{\mu\nu}^{3/2}(k_1, m_Y, \Gamma_Y)\right]\left[\frac{f_{pY_{3/2^+}K}}{m_\pi}(-ip_1^\nu)\right]u(p_2, m_2)F(q_i^2, \Lambda_a^2)F(q_f^2, \Lambda_a^2), \\ \mathcal{M}_{Y_{3/2^+}}^u &= \bar{u}_\mu(p_4, m_4)\left[-if_{\Xi'Y_{3/2^+}K}\gamma_5\right]\left[S_{\mu\nu}^{3/2}(k_1, m_Y, \Gamma_Y)\right]\left[\frac{f_{pY_{3/2^+}K}}{m_\pi}(ip_3^\nu)\right]u(p_2, m_2)F(q_i^2, \Lambda_a^2)F(q_f^2, \Lambda_a^2), \\ \mathcal{M}_{Y_{3/2^-}}^s &= \bar{u}_\mu(p_4, m_4)\left[if_{\Xi'Y_{3/2^-}K}\right]\left[S_{\mu\nu}^{3/2}(k_1, m_Y, \Gamma_Y)\right]\left[\frac{f_{pY_{3/2^-}K}}{m_\pi}\gamma_5(-ip_1^\nu)\right]u(p_2, m_2)F(q_i^2, \Lambda_a^2)F(q_f^2, \Lambda_a^2), \\ \mathcal{M}_{Y_{3/2^-}}^u &= \bar{u}_\mu(p_4, m_4)\left[if_{\Xi'Y_{3/2^-}K}\right]\left[S_{\mu\nu}^{3/2}(k_1, m_Y, \Gamma_Y)\right]\left[\frac{f_{pY_{3/2^-}K}}{m_\pi}\gamma_5(ip_3^\nu)\right]u(p_2, m_2)F(q_i^2, \Lambda_a^2)F(q_f^2, \Lambda_a^2), \\ \mathcal{M}_{Y_{5/2^+}}^s &= \bar{u}_{\mu_1}(p_4, m_4)\left[\frac{f_{\Xi'Y_{5/2^+}K}}{m_\pi}(ip_3^{\mu_2})\right]\left[S_{\mu_1\nu_1\mu_2\nu_2}^{5/2}(k_1, m_Y, \Gamma_Y)\right]\left[-i\frac{f_{pY_{5/2^+}K}}{m_\pi^2}\gamma_5(-p_1^{\nu_1}p_1^{\nu_2})\right]u(p_2, m_2)F(q_i^2, \Lambda_b^2)F(q_f^2, \Lambda_b^2), \\ \mathcal{M}_{Y_{5/2^+}}^u &= \bar{u}_{\mu_1}(p_4, m_4)\left[\frac{f_{\Xi'Y_{5/2^+}K}}{m_\pi}(-ip_1^{\mu_2})\right]\left[S_{\mu_1\nu_1\mu_2\nu_2}^{5/2}(k_1, m_Y, \Gamma_Y)\right]\left[-i\frac{f_{pY_{5/2^+}K}}{m_\pi^2}\gamma_5(-p_3^{\nu_1}p_3^{\nu_2})\right]u(p_2, m_2)F(q_i^2, \Lambda_b^2)F(q_f^2, \Lambda_b^2), \\ \mathcal{M}_{Y_{5/2^-}}^s &= \bar{u}_{\mu_1}(p_4, m_4)\left[\frac{f_{\Xi'Y_{5/2^-}K}}{m_\pi}\gamma_5(ip_3^{\mu_2})\right]\left[S_{\mu_1\nu_1\mu_2\nu_2}^{5/2}(k_1, m_Y, \Gamma_Y)\right]\left[-i\frac{f_{pY_{5/2^-}K}}{m_\pi^2}(-p_1^{\nu_1}p_1^{\nu_2})\right]u(p_2, m_2)F(q_i^2, \Lambda_b^2)F(q_f^2, \Lambda_b^2), \\ \mathcal{M}_{Y_{5/2^-}}^u &= \bar{u}_{\mu_1}(p_4, m_4)\left[\frac{f_{\Xi'Y_{5/2^-}K}}{m_\pi}\gamma_5(-ip_1^{\mu_2})\right]\left[S_{\mu_1\nu_1\mu_2\nu_2}^{5/2}(k_1, m_Y, \Gamma_Y)\right]\left[-i\frac{f_{pY_{5/2^-}K}}{m_\pi^2}(-p_3^{\nu_1}p_3^{\nu_2})\right]u(p_2, m_2)F(q_i^2, \Lambda_b^2)F(q_f^2, \Lambda_b^2),\end{aligned}\quad (5)$$

where the superscripts s, u correspond to s - and u -channel, respectively, and the subscript Y_{J^P} corresponds to hyperon involved in the processes. In the above amplitudes, the $S^{1/2}(k_i, m_i, \Gamma_i)$ refers to the propagator corresponding to the baryon with spin 1/2, which is [32],

$$S^{1/2}(k_i, m_i, \Gamma_i) = \frac{k_i + m_i}{k_i^2 - m_i^2 + im_i\Gamma_i}, \quad (6)$$

and $S_{\mu\nu}^{3/2}(k_i, m_i, \Gamma_i)$ is the propagator corresponding to the baryon with spin 3/2, which reads,

$$\begin{aligned}S_{\mu\nu}^{3/2}(k_i, m_i, \Gamma_i) &= \frac{k_i + m_i}{k_i^2 - m_i^2 + im_i\Gamma_i}\left(-g^{\mu\nu} + \frac{1}{3}\gamma^\mu\gamma^\nu\right. \\ &\quad \left.+ \frac{2p^\mu p^\nu}{3m_i^2} + \frac{\gamma^\mu p^\nu - p^\mu \gamma^\nu}{3m_i}\right).\end{aligned}\quad (7)$$

TABLE I: The resonance parameters of the involved Λ and Σ hyperon and their resonances.

State	J^P	Mass (MeV)	Width (MeV)
$\Lambda(1116)$	$1/2^+$	1116	—
$\Lambda(1405)$	$1/2^-$	1405	50
$\Lambda(1890)$	$3/2^+$	1890	120
$\Lambda(2110)$	$5/2^+$	2090	250
$\Lambda(2325)$	$3/2^-$	2325	170
$\Sigma(1193)$	$1/2^+$	1193	—
$\Sigma(1670)$	$3/2^-$	1662	55
$\Sigma(2080)$	$3/2^+$	2090	170
$\Sigma(2250)$	$5/2^-$	2250	100

The $S_{\mu_1\mu_2\nu_1\nu_2}^{5/2}(k_i, m_i, \Gamma_i)$ is the propagator corresponding to the baryon with spin 5/2, and its detailed expression is [33],

$$\begin{aligned}
S_{\mu_1\mu_2\nu_1\nu_2}^{5/2}(k_i, m_i, \Gamma_i) = & \frac{k_i + \sqrt{s}}{10(k_i^2 - m_i^2 + im_i\Gamma_i)} \\
& \times \left(5P_{\mu_1\mu_2}P_{\nu_1\nu_2} - 2P_{\mu_1\nu_1}P_{\mu_2\nu_2} \right. \\
& + 5P_{\mu_1\nu_2}P_{\nu_1\mu_2} + P_{\mu_1\rho}\gamma^\rho\gamma^\sigma P_{\sigma\mu_2}P_{\nu_1\nu_2} \\
& + P_{\nu_1\rho}\gamma^\rho\gamma^\sigma P_{\sigma\nu_2}P_{\mu_1\mu_2} + P_{\mu_1\rho}\gamma^\rho\gamma^\sigma P_{\sigma\nu_2}P_{\nu_1\mu_2} \\
& \left. + P_{\nu_1\rho}\gamma^\rho\gamma^\sigma P_{\rho\mu_2}P_{\mu_1\nu_2} \right), \quad (8)
\end{aligned}$$

with

$$P_{\mu\nu} = -g_{\mu\nu} + q_\mu q_\nu / s. \quad (9)$$

In addition, two form factors are introduced to depict the two relevant vertices, and both form factors are in the same form, which is

$$F(\vec{q}^2, \Lambda_i^2) = \exp(-\vec{q}^2 / \Lambda_i^2), \quad (10)$$

where Λ_i stands for the cutoff constant. In the present estimations, we adopt two different values of Λ_i , which is Λ_a for low-spin propagator ($J^P \leq 3/2$) and Λ_b for high-spin propagator ($J \geq 5/2$) as in Ref. [31]. In addition, \vec{q}_i and \vec{q}_f stand for three-momentum of the initial K^- and the final K^+ in the center-of-mass system, respectively, which read,

$$\begin{aligned}
\vec{q}_i &= \sqrt{\frac{(s - (m_1 - m_2)^2)(s - (m_1 + m_2)^2)}{4s}}, \\
\vec{q}_f &= \sqrt{\frac{(s - (m_3 - m_4)^2)(s - (m_3 + m_4)^2)}{4s}}. \quad (11)
\end{aligned}$$

In the same way, one can investigate the $\Xi(1530)^0$ production in the K^-p scattering process, and the relevant diagrams are shown in Fig. 2. It should be noted that in the

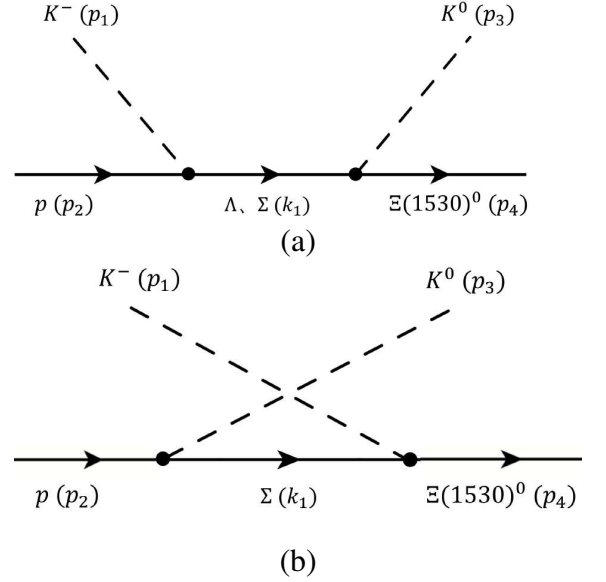


FIG. 2: Diagrams contributing to the process $K^-p \rightarrow K^0\Xi(1530)^0$, in which (a) and (b) correspond to the s - and u -channel contributions, respectively.

u -channel, the exchanged hyperons should only be Σ and its resonances, while Λ hyperon and its resonances are forbidden due to charge conservation. Thus, from the isospin symmetry, the contributions from Σ hyperon and its resonances are the same in both $K^-p \rightarrow K^+\Xi(1530)^-$ and $K^-p \rightarrow K^0\Xi(1530)^0$ processes, while those from Λ hyperon and its resonances are different in both processes.

III. NUMERICAL RESULTS AND DISCUSSIONS

To describe the experimental data of the cross sections for $K^-p \rightarrow K^+\Xi(1530)^-$ and $K^-p \rightarrow K^0\Xi(1530)^0$ [16, 22, 27, 28], we have considered nine Λ/Σ hyperon and their resonances as intermediate states and the involved states are presented in Table I. For the resonances with high-spin, i.e., $\Lambda(2110)$ and $\Sigma(2250)$, only s -channels are considered as in Ref. [31]. Therefore, the amplitude for $K^-p \rightarrow K^+\Xi(1530)^-$ reads,

$$\begin{aligned}
\mathcal{M}_{K^+\Xi^-}^{\text{Tot}} = & \mathcal{M}_{\Lambda(1116)}^s + \mathcal{M}_{\Lambda(1116)}^u + \mathcal{M}_{\Sigma(1193)}^s + \mathcal{M}_{\Sigma(1193)}^u \\
& + \mathcal{M}_{\Lambda(1405)}^s + \mathcal{M}_{\Lambda(1405)}^u + \mathcal{M}_{\Sigma(1670)}^s + \mathcal{M}_{\Sigma(1670)}^u \\
& + \mathcal{M}_{\Lambda(1890)}^s + \mathcal{M}_{\Lambda(1890)}^u + \mathcal{M}_{\Sigma(2080)}^s + \mathcal{M}_{\Sigma(2080)}^u \\
& + \mathcal{M}_{\Lambda(2110)}^s + \mathcal{M}_{\Lambda(2110)}^u + \mathcal{M}_{\Sigma(2250)}^s + \mathcal{M}_{\Sigma(2250)}^u \\
& + \mathcal{M}_{\Lambda(2325)}^s + \mathcal{M}_{\Lambda(2325)}^u. \quad (12)
\end{aligned}$$

Similarly, one can obtain the amplitudes for $K^-p \rightarrow K^0\Xi(1530)^0$, which is,

$$\begin{aligned}
\mathcal{M}_{K^0\Xi^0}^{\text{Tot}} = & \mathcal{M}_{\Lambda(1116)}^s + \mathcal{M}_{\Sigma(1193)}^s + \mathcal{M}_{\Sigma(1193)}^u + \mathcal{M}_{\Lambda(1405)}^s \\
& + \mathcal{M}_{\Sigma(1670)}^s + \mathcal{M}_{\Sigma(1670)}^u + \mathcal{M}_{\Lambda(1890)}^s + \mathcal{M}_{\Sigma(2080)}^s \\
& + \mathcal{M}_{\Sigma(2080)}^u + \mathcal{M}_{\Lambda(2110)}^s + \mathcal{M}_{\Sigma(2250)}^s + \mathcal{M}_{\Sigma(2250)}^u \\
& + \mathcal{M}_{\Lambda(2325)}^s. \quad (13)
\end{aligned}$$

With the above amplitudes, one can obtain the differential cross sections for the $K^-p \rightarrow K\Xi(1530)$, which is,

$$\frac{d\sigma}{d\cos\theta} = \frac{1}{32\pi s} \frac{|\vec{q}_f|}{|\vec{q}_i|} \left(\frac{1}{2} \left| \mathcal{M}_{K\Xi}^{\text{Tot}} \right|^2 \right), \quad (14)$$

where s refers to the square of the center-of-mass energy, and θ is the scattering angle, which is the angle of outgoing $\Xi(1530)$ and the incident kaon beam direction in the center-of-mass frame. The \vec{q}_f and \vec{q}_i stand for three-momentum of the final $\Xi(1530)$ and the initial kaon beam in the center-of-mass system, respectively, and their values are presented in Eqs. (11).

As indicated in Eqs. (5), the coupling constants $f_{\Xi'Y,pK}$ and $f_{pY,pK}$ always appear in the same amplitude, and the amplitude is proportional to the product of these two coupling constants. Thus, we can define the product of these two coupling constants as one single parameter, which is,

$$g_Y = f_{\Xi'YK} \times f_{pYK}, \quad (15)$$

where Y refers to the Λ/Σ hyperon and their resonances. In the present estimations, the values of g_Y will be determined by fitting the cross sections for $K^-p \rightarrow K^+\Xi(1520)^-$ and $K^-p \rightarrow K^0\Xi(1520)^0$.

A. Cross sections for $K^-p \rightarrow K\Xi(1530)$

In the present fitting process, nine Λ/Σ hyperon and their resonances are taken into consideration. In addition, two kinds of cutoff constants, Λ_a and Λ_b , are involved by the form factors in the amplitudes, with for low-spin intermediate states ($J^P \leq 3/2$) and Λ_b for high-spin intermediate states ($J \geq 5/2$), respectively. Here, we take $\Lambda_a = 1.0$ GeV and $\Lambda_b = 0.5$ GeV as in Ref. [31], while the rest parameters g_Y can be determined by fitting the cross sections for $K^-p \rightarrow K^+\Xi(1530)^-$ and $K^-p \rightarrow K^0\Xi(1530)^0$. In addition, it should be noted that the experimental data for the cross sections for $K^-p \rightarrow K^+\Xi(1530)^-$ in the range of $\sqrt{s} = [2.087, 2.168]$ GeV are inconsistent with each other as shown in Fig. 3. In particular, the cross sections at 2.087 GeV, 2.111 GeV, 2.123 GeV, 2.126 GeV, 2.151 GeV, and 2.168 GeV are around $80 \mu\text{b}$ with large uncertainties, while the cross section at 2.108 GeV is measured to be $(41 \pm 10) \mu\text{b}$, which is evidently smaller than the nearby data. Due to the inconsistency mentioned above, in the following, we perform the fitting with the experimental data having the same weight (model A) and different weight (model B).

1. Model A

In this scenario, the parameters g_Y determined by fitting the cross sections for $K^-p \rightarrow K^+\Xi(1530)^-$ and $K^-p \rightarrow K^0\Xi(1530)^0$ are collected in Table II. With the central values of the determined parameters, one has $\chi^2/d.o.f = 63.38/50 = 1.27$, which is acceptable for the present fit. In Fig. 3, we

TABLE II: The fitted parameters of the process $K^-p \rightarrow K\Xi(1530)$, where the weight of each experimental data remains the same.

Coupling constant	Value	Coupling constant	Value
$g_{\Lambda(1116)}$	$1.373^{+0.196}_{-0.196}$	$g_{\Sigma(1193)}$	$-3.178^{+0.068}_{-0.068}$
$g_{\Lambda(1405)}$	$-0.046^{+0.080}_{-0.080}$	$g_{\Sigma(1670)}$	$-1.545^{+0.195}_{-0.195}$
$g_{\Lambda(1890)}$	$0.496^{+0.267}_{-0.267}$	$g_{\Sigma(2080)}$	$-0.864^{+0.198}_{-0.198}$
$g_{\Lambda(2110)}$	$0.453^{+0.022}_{-0.022}$	$g_{\Sigma(2250)}$	$0.209^{+0.033}_{-0.033}$
$g_{\Lambda(2325)}$	$-0.182^{+0.017}_{-0.017}$		
$\chi^2 = 63.38$			

TABLE III: The fitted parameters of the process $K^-p \rightarrow K\Xi(1530)$, where increasing the weight (eight times) of six experimental data with high cross sections, and delete the one experimental data with low cross section in the range of $\sqrt{s} = [2.087, 2.168]$ GeV.

Coupling constant	Value	Coupling constant	Value
$g'_{\Lambda(1116)}$	$1.116^{+0.220}_{-0.220}$	$g'_{\Sigma(1193)}$	$-3.321^{+0.145}_{-0.145}$
$g'_{\Lambda(1405)}$	$-0.192^{+0.085}_{-0.085}$	$g'_{\Sigma(1670)}$	$-2.065^{+0.281}_{-0.281}$
$g'_{\Lambda(1890)}$	$0.187^{+0.600}_{-0.600}$	$g'_{\Sigma(2080)}$	$-0.805^{+0.217}_{-0.217}$
$g'_{\Lambda(2110)}$	$0.545^{+0.015}_{-0.015}$	$g'_{\Sigma(2250)}$	$0.212^{+0.034}_{-0.034}$
$g'_{\Lambda(2325)}$	$-0.197^{+0.015}_{-0.015}$		
$\chi_0^2 = 96.29$		$\chi_1^2 = 138.93$	

present the fitted cross sections for $K^-p \rightarrow K^+\Xi(1530)^-$ (diagram (a)) and $K^-p \rightarrow K^0\Xi(1530)^0$ (diagram (b)), where the experimental data from Refs. [16, 22, 27, 28] are also presented for comparison. From the figure one can find that the cross sections for $K^-p \rightarrow K^0\Xi(1530)^0$ (diagram (b)) can be well reproduced in the whole considered range. Meanwhile, the cross sections for $K^-p \rightarrow K^+\Xi(1530)^-$ can also be reproduced except for the data in the range of $\sqrt{s} = [2.087, 2.168]$ GeV due to the inconsistency of the experimental data. Particularly, the cross section for $K^-p \rightarrow K^+\Xi(1530)^-$ is fitted to be $50.41 \mu\text{b}$ at $\sqrt{s} = 2.11$ GeV, which is consistent with the experimental measurement within uncertainty. However, the fitted cross sections in the range of $\sqrt{s} = [2.087, 2.168]$ GeV are in whole smaller than other data in this range. Furthermore, it is worth noting that there are two clear peak structures around $\sqrt{s} = 2.1$ GeV and $\sqrt{s} = 2.3$ GeV in both cross sections.

In addition to the total cross sections, the individual contributions of each intermediate state for $K^-p \rightarrow K^+\Xi(1530)^-$ are presented in Fig. 4. From Fig. 4-(a) one can find that the cross sections resulted from $\Sigma(1193)$ intermediate process are predominant, while the cross section resulted from $\Lambda(1116)$ is several times smaller than that of $\Sigma(1193)$. As indicated

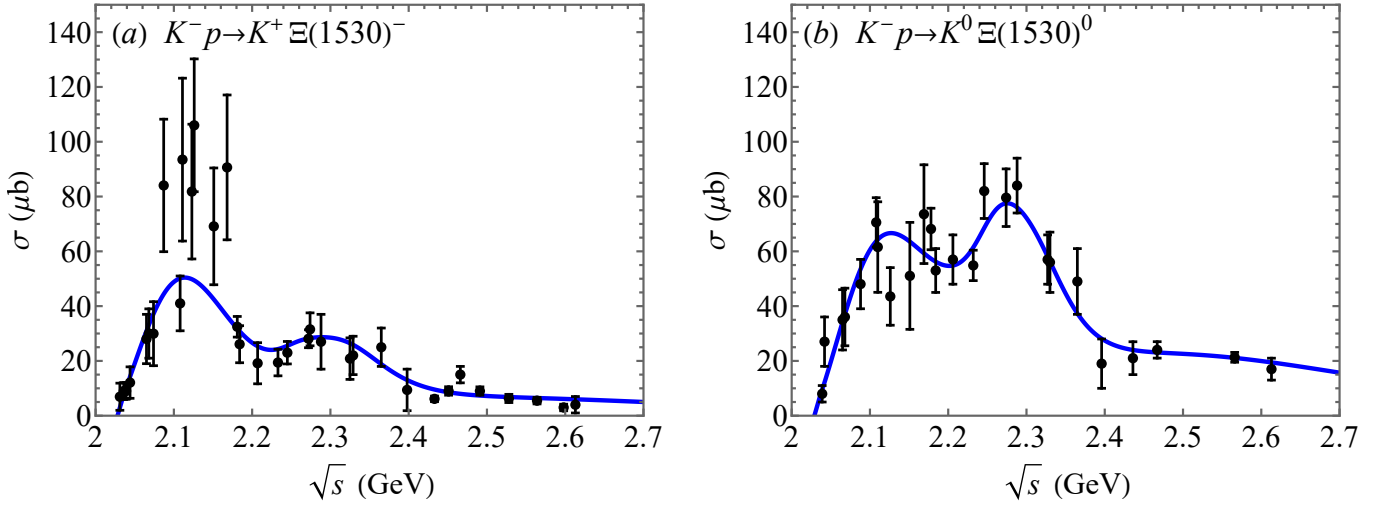


FIG. 3: (Color online) The cross sections for the $K^-p \rightarrow K^+\Xi(1530)^-$ (diagram (a)) and $K^-p \rightarrow K^0\Xi(1530)^0$ (diagram (b)) processes depending on the \sqrt{s} . The black points with error bars correspond to the experimental data for $K^-p \rightarrow K\Xi(1530)$ from Ref. [16, 22, 27, 28], while the blue solid curves are obtained with the fitted parameters in Table II.

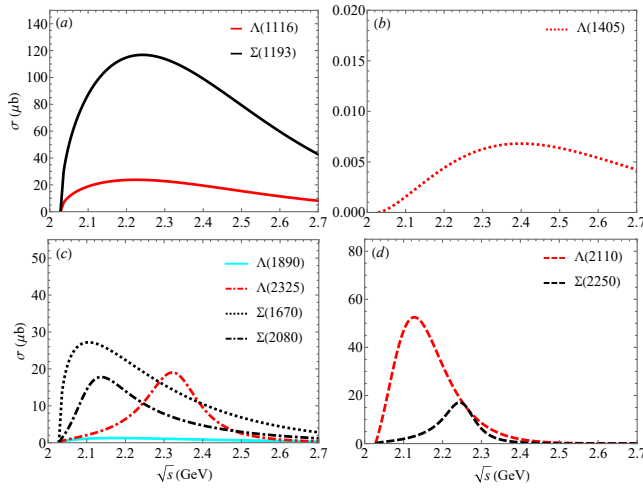


FIG. 4: (Color online) The individual contributions from different intermediate states for the cross sections for $K^-p \rightarrow K^+\Xi(1530)^-$ depending on the \sqrt{s} in Model A.

by Fig. 4-(b), the cross sections resulted from $\Lambda(1405)$ are at least 3 orders smaller than those from $\Lambda(1116)$, which indicate that the contributions from $\Lambda(1405)$ are negligible even if one considers the interference contributions with other states. In Fig. 4-(c), we present the contributions from $\Lambda(1890)$, $\Lambda(2325)$, $\Sigma(1670)$, and $\Sigma(2080)$, whose total angular momenta are $3/2$. From this diagram, one can find that the contribution from $\Lambda(1890)$ is not obvious with its contribution to the cross sections to be less than $2 \mu\text{b}$. Meanwhile, the peak values of cross sections for $\Lambda(2325)$, $\Sigma(1670)$, and $\Sigma(2080)$ are about $20 \sim \mu\text{b}$. In Fig. 4-(d), we present the individual contributions from two high-spin intermediate state, i.e. $\Lambda(2110)$ and $\Sigma(2250)$. The maximum of the cross sections resulted from $\Lambda(2110)$ is estimated to be around $50 \mu\text{b}$ at $\sqrt{s} = 2.13$ GeV,

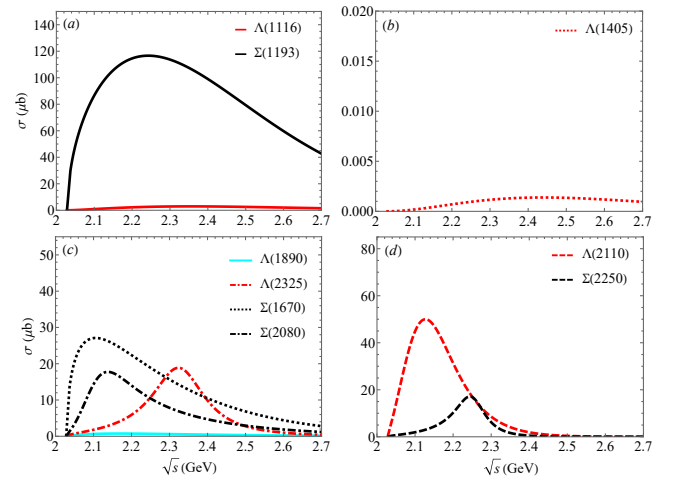


FIG. 5: (Color online) The individual contributions from different intermediate states for the cross sections for $K^-p \rightarrow K^0\Xi(1530)^0$ depending on the \sqrt{s} in Model A.

and the contribution from $\Sigma(2250)$ is about $1/3$ of that from $\Lambda(2110)$ in the peak position.

In addition, the individual contributions from hyperon for $K^-p \rightarrow K^0\Xi(1530)^0$ are presented in Fig. 5. Comparing with Fig. 4, one can find that the cross sections resulted from four Σ intermediate states are basically consistent in these two processes, which is consistent with isospin symmetry expectation. As for Λ intermediate process, the u -channel contributions vanish for the $K^-p \rightarrow K^0\Xi(1530)^0$ process due to charge conservation. Comparing Fig. 4 and Fig. 5, one can find that the contributions from $\Lambda(1116)$, $\Lambda(1405)$ and $\Lambda(1890)$ are much larger in $K^-p \rightarrow K^+\Xi(1530)^-$ process, which indicates that the u -channel is dominant for the below threshold intermediate states. Moreover, the contributions from the above

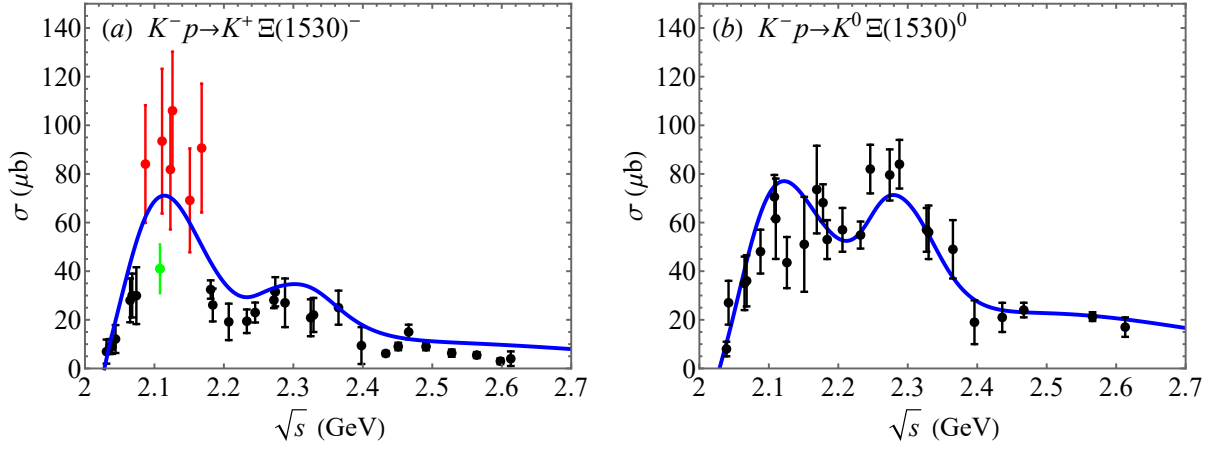


FIG. 6: (Color online) The same as Fig. 3 but for the weighted fit. The points with error bars correspond to the experimental data for $K^-p \rightarrow K\Xi(1530)$ from Ref. [16, 22, 27, 28], while the blue solid curves are obtained with the fitted parameters in Table III. The green data are excluded in the present fit, while the weight of the six red data in the range of $\sqrt{s} = [2.087, 2.168]$ GeV are set to 8.

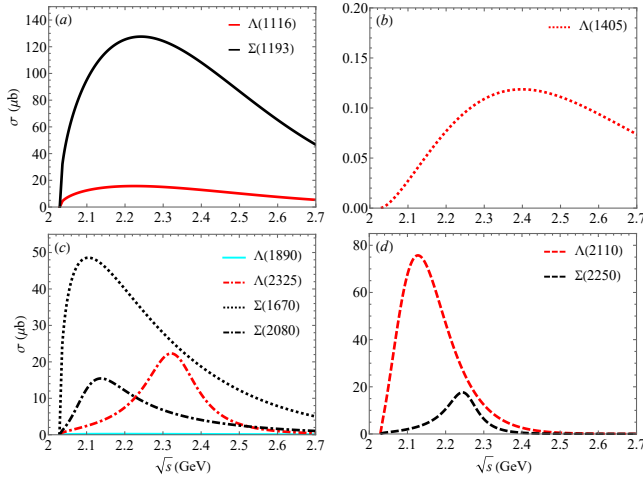


FIG. 7: (Color online) The same as Fig. 4 but in Model B.

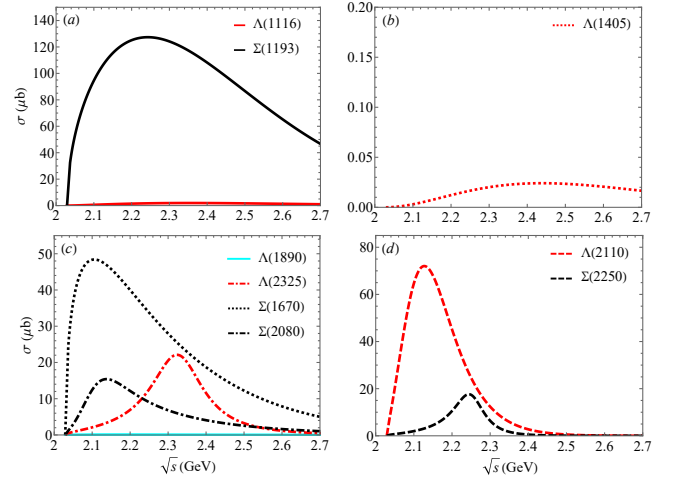


FIG. 8: (Color online) The same as Fig. 5 but in Model B.

threshold Λ resonances, such as $\Lambda(2110)$ and $\Lambda(2325)$ are similar, indicating that the s -channel is dominant.

2. Model B

As we clarified at the beginning of this subsection, the experimental data for the cross sections for $K^-p \rightarrow K^+\Xi(1530)^-$ in the range of $\sqrt{s} = [2.087, 2.168]$ GeV are inconsistent with each other. In Model B, we first remove the data at $\sqrt{s} = 2.11$ GeV and perform a weighted fit with the weights of the other data in the range enhanced. For example, when we set the weight of these data to 8, we can obtain the line shape of the cross sections for $K^-p \rightarrow K^+\Xi(1530)^-$ and reproduce the data in the range of $\sqrt{s} = [2.087, 2.168]$ GeV. In this case the fitted parameters are collected in Table II. With these parameters, the χ^2 and weight χ^2 is estimated to be 96.24 and 138.93, which are much larger than those in model A.

Using the parameters in Table II, we can obtain the cross sections for $K^-p \rightarrow K^+\Xi(1530)^-$ and $K^-p \rightarrow K^0\Xi(1530)^0$, which are presented in Fig. 6. Notably, the cross sections for $K^-p \rightarrow K^+\Xi(1530)^-$ approach $70 \mu\text{b}$ in the vicinity of 2.1 GeV, which are consistent with the lower limit of the experimental data. Nonetheless, the fitted cross sections overestimate the experimental measurements outside the range of $\sqrt{s} = [2.087, 2.168]$ GeV. For the $K^-p \rightarrow K^0\Xi(1530)^0$ process, the fitted curve exhibits a modest overestimation of the experimental data in the vicinity of 2.1 GeV, followed by an underestimation around 2.3 GeV. Based on a comparative analysis of Figs. 4 and 6, we conclude that Model A demonstrates a better global agreement with the experimental data than Model B.

In Figs. 7 and 8, we present the individual contributions from different intermediate states for $K^-p \rightarrow K^+\Xi(1530)^-$ and $K^-p \rightarrow K^0\Xi(1530)^0$, respectively. From the individual contributions, one can find that the resonances $\Sigma(2080)$,

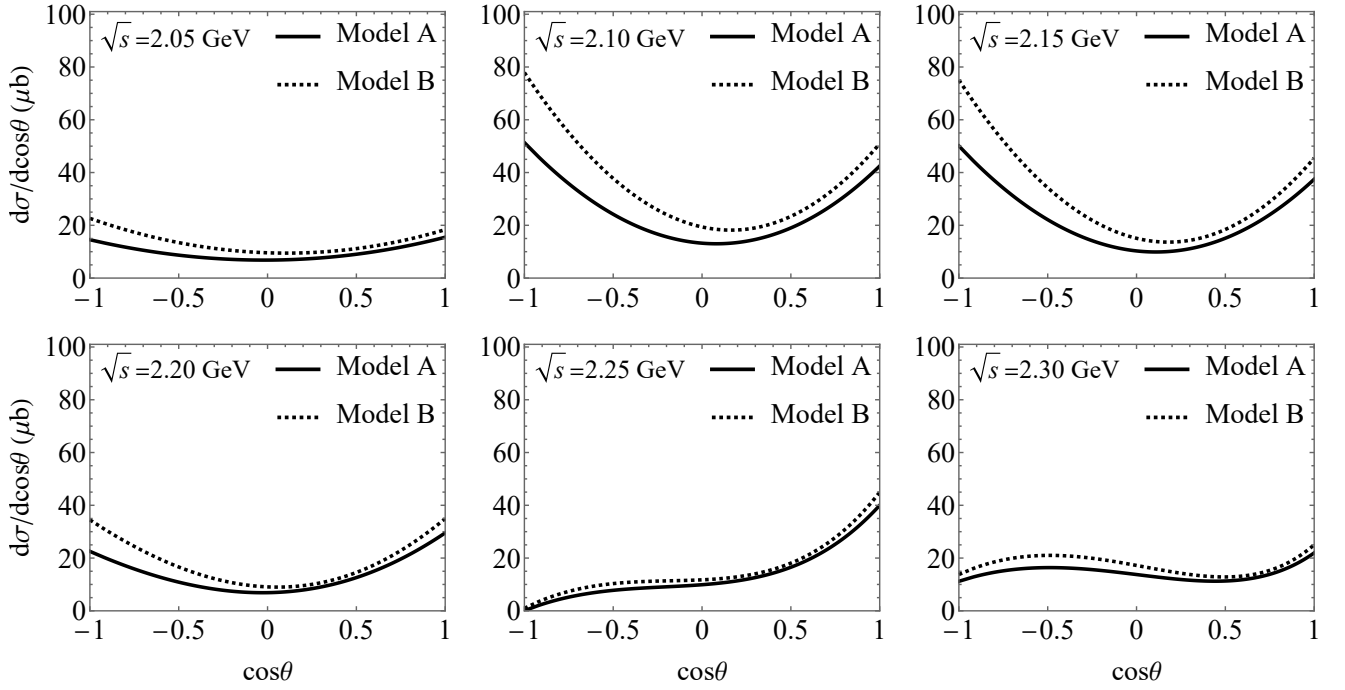


FIG. 9: (Color online) The differential cross sections for $K^-p \rightarrow K^+\Xi(1530)^-$ depending on $\cos\theta$ with several typical values of \sqrt{s} . The black solid curves are obtained with the fitted parameters in Table II, which correspond to Model A. The black dotted curves are obtained with the fitted parameters in Table III, which correspond to Model B.

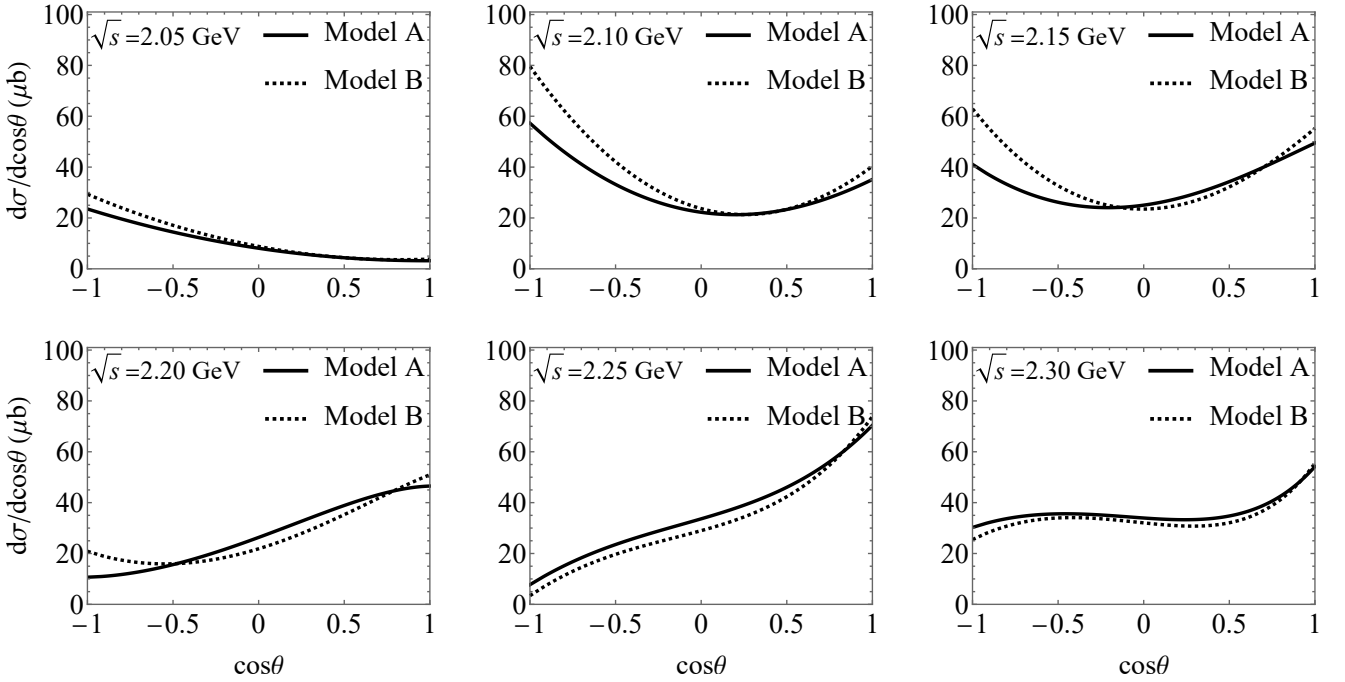


FIG. 10: (Color online) The same as Fig. 9 but for the process $K^-p \rightarrow K^0\Xi(1530)^0$.

$\Sigma(1670)$ and $\Lambda(2110)$ significantly contribute to the peak structure around 2.1 GeV. In order to enhance the cross sections for $K^-p \rightarrow K^+\Xi(1530)^-$ in the vicinity of 2.1 GeV, the contributions from these resonances should be increased. By comparing the fitted parameters in Tables II and III, one

can find that in Model B the absolute value of the parameters $g_{\Sigma(1670)}$ and $g_{\Lambda(2110)}$ increase by 33.6% and 20.0%, respectively, while the absolute value of $g_{\Sigma(2080)}$ decreases by 6.8%. However, as we analyzed in Model A, the contributions for Σ resonances are the same for $K^-p \rightarrow K^+\Xi(1530)^-$

and $K^-p \rightarrow K^0\Xi(1530)^0$. In addition, the contributions from above threshold Λ resonance are s -channel dominant, indicating the above threshold Λ resonances have similar contributions to $K^-p \rightarrow K^+\Xi(1530)^-$ and $K^-p \rightarrow K^0\Xi(1530)^0$ processes. Thus, the overall enhancement of the cross sections for $K^-p \rightarrow K^+\Xi(1530)^-$ in the vicinity of 2.1 GeV inevitably also enhance the cross sections for $K^-p \rightarrow K^0\Xi(1530)^0$, which lead to a worse global agreement with the experimental data of the cross sections for $K^-p \rightarrow K^0\Xi(1530)^0$ near 2.1 GeV.

B. Predictions of the differential cross sections for $K^-p \rightarrow K\Xi(1530)$

In addition to the cross sections, the differential cross sections for the involved processes depending on $\cos\theta$ are predicted with the fitted parameters in the present work, where θ is the angle between the outgoing $\Xi(1530)$ and the ingoing kaon beam direction. The differential cross sections with several typical center-of-mass energies for $K^-p \rightarrow K^+\Xi(1530)^-$ and $K^-p \rightarrow K^0\Xi(1530)^0$ are presented in Figs. 9 and 10, respectively. Here, we take the center-of-mass energy \sqrt{s} as 2.05, 2.10, 2.15, 2.20, 2.25, 2.30 GeV, respectively. From the figure one can notice that the differential cross sections reach the maximum at the backward angle limit when $\sqrt{s} = 2.10$ and 2.15 GeV, while when $\sqrt{s} = 2.25$ GeV, the differential cross sections reach its maximum at the forward angle limit. In addition, by comparing Model A and Model B, one can find that the differential cross sections of Model B are generally greater than that of Model A, which are consistent with the relevant cross sections. Moreover, the differential cross sections for $K^-p \rightarrow K^0\Xi(1530)^0$ are presented in Fig. 10. Similarly, the black solid curves and black dotted curves correspond to Model A and Model B, respectively. In most cases, the differential cross sections are similar for $K^-p \rightarrow K^+\Xi(1530)^-$ and $K^-p \rightarrow K^0\Xi(1530)^0$, since the contributions from the Σ hyperon are the same for both processes, and those from above threshold Λ hyperon are also similar. These differential cross sections predicted in the present work could be crucial tests to the present estimations, which should be accessible by the kaon experiments at J-PARC.

C. Cross sections for $K^-p \rightarrow K\Xi\pi$ at $p_K = 2.87$ GeV

Since the $\Xi(1530)^-$ and $\Xi(1530)^0$ states can further decay into $\Xi^-\pi^0$ and $\Xi^-\pi^+$, respectively, one can estimate the cross sections for the cascade processes $K^-p \rightarrow K^+\Xi(1530)^- \rightarrow K^+\Xi^-\pi^0$ and $K^-p \rightarrow K^0\Xi(1530)^0 \rightarrow \Xi^-\pi^+$. Experimentally, the authors of Ref. [27] measured the cross sections for $K^-p \rightarrow K^+\Xi^-\pi^0$ and $K^-p \rightarrow K^0\Xi^-\pi^+$ to be $(5.5 \pm 1.4) \mu\text{b}$ and $(14.2 \pm 1.8) \mu\text{b}$ at $p_K = 2.87$ GeV (equivalent to $\sqrt{s} = 2.57$ GeV), respectively, where $\Xi^-\pi^0$ and $\Xi^-\pi^+$ are the daughter particles of $\Xi(1530)^-$ and $\Xi(1530)^0$, respectively. Considering the isospin symmetry, the branching ratios of $\Xi(1530)^- \rightarrow \Xi^-\pi^0$ and $\Xi(1530)^0 \rightarrow \Xi^-\pi^+$ are about 33.3% and 66.6%, respectively [28]. Then, by combining the cross sections for the two-body processes that have already been obtained in Section

III, one can predict the cross sections for the three-body processes. For Model A, Our estimations indicate that the cross sections for $K^-p \rightarrow K^+\Xi(1530)^-$ and $K^-p \rightarrow K^0\Xi(1530)^0$ are about $6.40 \mu\text{b}$ and $20.98 \mu\text{b}$ at $\sqrt{s} = 2.57$ GeV, respectively. Therefore, the cross sections for the charged and neutral three-body processes can be approximately estimated to be $2 \mu\text{b}$ and $14 \mu\text{b}$ at $\sqrt{s} = 2.57$ GeV, respectively. For Model B, Our estimations indicate that the cross sections for $K^-p \rightarrow K^+\Xi(1530)^-$ and $K^-p \rightarrow K^0\Xi(1530)^0$ are about $10.14 \mu\text{b}$ and $21.52 \mu\text{b}$ at $\sqrt{s} = 2.57$ GeV, respectively. Consequently, the cross sections for the charged and neutral three-body processes are about $3 \mu\text{b}$ and $14 \mu\text{b}$ at $\sqrt{s} = 2.57$ GeV, respectively. To sum up, the estimated results in the present fit are basically consistent with the experimental measurements for the three-body process for both model.

IV. SUMMARY

The ground Ξ hyperon state, $\Xi(1314)$ has been comprehensively studied over the years, and the researches on its productions in the K^-p scattering processes have been performed in the literature. However, the researches on the productions of $\Xi(1530)$ are limited due to the scarcity of the experimental data. In the present work, we investigate the production of $\Xi(1530)^0$ and $\Xi(1530)^-$ in the K^-p scattering process simultaneously, where nine Λ/Σ hyperons and their resonances are involved in the s - and u -channel processes. Checking the experimental data, we find that the measured cross sections for $K^-p \rightarrow K^+\Xi(1530)^-$ are inconsistent with each other in the range $\sqrt{s} = [2.087, 2.168]$ GeV. Thus, in the present work, we take two different strategies. In Model A, the weight of the experimental data are the same, while in Model B, the experimental data have different weight. Based on a comparative analysis of the fit results in two models, we conclude that Model A demonstrates a better global agreement with the experimental data than Model B.

In addition to the cross sections, the individual contributions from different intermediate states to the cross sections for $K^-p \rightarrow K^+\Xi(1530)^-$ and $K^-p \rightarrow K^0\Xi(1530)^0$ are also estimated with the fitted parameters. Our results indicate that the cross section resulted from $\Sigma(1193)$ intermediate process is predominant. Moreover, the different cross sections are predicted for both the charged and neutral processes with several typical center-of-mass energies, which could be tested by further experimental measurements at J-PARC in the future.

ACKNOWLEDGMENTS

This work is partly supported by the National Natural Science Foundation of China under the Grant Nos. 12175037 and 12335001, as well as supported, in part, by National Key Research and Development Program under the contract No. 2024YFA1610503. PW acknowledges support from Natural Science Foundation of Jiangsu Province (Grant No. BK20210201), Fundamental Research Funds for the Central Universities, Excellent Scholar Project of Southeast Univer-

-
- [1] S. Navas *et al.* [Particle Data Group], Review of particle physics, Phys. Rev. D **110**, no.3, 030001 (2024) doi:10.1103/PhysRevD.110.030001
- [2] D. H. Lyth and D. Wands, Generating the curvature perturbation without an inflaton, Phys. Lett. B **524**, 5-14 (2002) doi:10.1016/S0370-2693(01)01366-1 [arXiv:hep-ph/0110002 [hep-ph]].
- [3] B. Aubert *et al.* [BaBar], Measurement of the Spin of the $\Xi(1530)$ Resonance, Phys. Rev. D **78**, 034008 (2008) doi:10.1103/PhysRevD.78.034008 [arXiv:0803.1863 [hep-ex]].
- [4] M. Sumihama *et al.* [Belle], Observation of $\Xi(1620)^0$ and evidence for $\Xi(1690)^0$ in $\Xi_c^+ \rightarrow \Xi^- \pi^+ \pi^+$ decays, Phys. Rev. Lett. **122**, no.7, 072501 (2019) doi:10.1103/PhysRevLett.122.072501 [arXiv:1810.06181 [hep-ex]].
- [5] J. W. Price *et al.* [CLAS], Exclusive photoproduction of the cascade Ξ hyperons, Phys. Rev. C **71**, 058201 (2005) doi:10.1103/PhysRevC.71.058201 [arXiv:nucl-ex/0409030 [nucl-ex]].
- [6] J. W. Price *et al.* [CLAS], Photoproduction of the doubly strange Ξ hyperons, Nucl. Phys. A **754**, 272-280 (2005) doi:10.1016/j.nuclphysa.2005.02.075 [arXiv:nucl-ex/0402006 [nucl-ex]].
- [7] L. Guo, D. P. Weygand, M. Battaglieri, R. D. Vita, V. Kubarovskiy, P. Stoler, M. J. Amarian, P. Ambrozewicz, M. Anghinolfi and G. Asryan, *et al.* Cascade production in the reactions $\gamma p \rightarrow K^+ K^+(X)$ and $\gamma p \rightarrow K^+ K^- \pi^-(X)$, Phys. Rev. C **76**, 025208 (2007) doi:10.1103/PhysRevC.76.025208 [arXiv:nucl-ex/0702027 [nucl-ex]].
- [8] S. Capstick and N. Isgur, Baryons in a relativized quark model with chromodynamics, Phys. Rev. D **34**, no.9, 2809-2835 (1986) doi:10.1103/physrevd.34.2809
- [9] K. T. Chao, N. Isgur and G. Karl, Strangeness -2 and -3 Baryons in a Quark Model With Chromodynamics, Phys. Rev. D **23**, 155 (1981) doi:10.1103/PhysRevD.23.155
- [10] L. Y. Glozman and D. O. Riska, The Spectrum of the nucleons and the strange hyperons and chiral dynamics, Phys. Rept. **268**, 263-303 (1996) doi:10.1016/0370-1573(95)00062-3 [arXiv:hep-ph/9505422 [hep-ph]].
- [11] L. Y. Xiao and X. H. Zhong, Ξ baryon strong decays in a chiral quark model, Phys. Rev. D **87**, no.9, 094002 (2013) doi:10.1103/PhysRevD.87.094002 [arXiv:1302.0079 [hep-ph]].
- [12] M. Pervin and W. Roberts, Strangeness -2 and -3 baryons in a constituent quark model, Phys. Rev. C **77**, 025202 (2008) doi:10.1103/PhysRevC.77.025202 [arXiv:0709.4000 [nucl-th]].
- [13] R. Bijker, F. Iachello and A. Leviatan, Algebraic models of hadron structure. 2. Strange baryons, Annals Phys. **284**, 89-133 (2000) doi:10.1006/aphy.2000.6064 [arXiv:nucl-th/0004034 [nucl-th]].
- [14] C. L. Schat, J. L. Goity and N. N. Scoccola, Masses of the 70-baryons in large N_c QCD, Phys. Rev. Lett. **88**, 102002 (2002) doi:10.1103/PhysRevLett.88.102002 [arXiv:hep-ph/0111082 [hep-ph]].
- [15] Y. Oh, Ξ and Ω baryons in the Skyrme model, Phys. Rev. D **75**, 074002 (2007) doi:10.1103/PhysRevD.75.074002 [arXiv:hep-ph/0702126 [hep-ph]].
- [16] J. P. Berge, P. Eberhard, J. R. Hubbard, D. W. Merrill, J. Button-Shafer, F. T. Solmitz and M. L. Stevenson, Some Properties of Ξ^- and Ξ^0 Hyperons Produced in $K^- p$ Interactions between 1.05 and 1.7 BeV/c, Phys. Rev. **147**, 945-961 (1966) doi:10.1103/PhysRev.147.945
- [17] G. W. London, R. R. Rau, N. P. Samios, S. S. Yamamoto, M. Goldberg, S. Lichtman, M. Prime and J. Leitner, $K^- - p$ Interaction at 2. Be-24Vc, Phys. Rev. **143**, 1034-1091 (1966) doi:10.1103/PhysRev.143.1034
- [18] M. Haque *et al.* [Birmingham-Glasgow-London(I.C.)-Oxford-Rutherford], Reactions $K^- p \rightarrow$ Hyperon + Meson at 3.5 GeV/c, Phys. Rev. **152**, 1148-1161 (1966) doi:10.1103/PhysRev.152.1148
- [19] T. G. Trippe and P. E. Schlein, Partial-Wave Analysis of $K^- p \rightarrow \Xi^- K^+$ at 2 GeV/c, Phys. Rev. **158**, no.5, 1334-1337 (1967) doi:10.1103/PhysRev.158.1334
- [20] W. P. Trower, J. R. Ficenec, R. I. Hulsizer, J. Lathrop, J. N. Snyder and W. P. Swanson, Some Two-Body Final States of $K^- p$ Interactions at 1.33 GeVc, Phys. Rev. **170**, 1207-1222 (1968) doi:10.1103/PhysRev.170.1207
- [21] G. Burgun, J. Meyer, E. Pauli, B. Tallini, J. Vrana, A. De Bellefon, A. Berthon, K. L. Rangan, J. Beaney and S. M. Deen, *et al.* Resonance formation in the reactions $K^- p \rightarrow K^+ \Xi^-$ and $K^- p \rightarrow K^0 \Xi^0$ in the mass region from 1915 to 2168 Mev, Nucl. Phys. B **8**, 447-459 (1968) doi:10.1016/0550-3213(68)90256-3
- [22] P. M. Dauber, J. P. Berge, J. R. Hubbard, D. W. Merrill and R. A. Muller, Production and decay of cascade hyperons, Phys. Rev. **179**, 1262-1285 (1969) doi:10.1103/PhysRev.179.1262
- [23] J. C. Scheuer *et al.* [SABRE], Experimental study of two-body and quasi-two-body reactions in $K^- n$ interactions at 3 GeV/c, Nucl. Phys. B **33**, 61-83 (1971) doi:10.1016/0550-3213(71)90387-7
- [24] A. de Bellefon, A. Berthon, L. K. Rangan, J. Vrana, T. C. Bacon, A. Brandstetter, I. Butterworth, S. M. Deen, C. M. Fisher and P. J. Litchfield, *et al.* Channel cross-sections of $K^- p$ reactions from 1.26 to 1.84 GeV/c, Nuovo Cim. A **7**, 567-583 (1972) doi:10.1007/BF02734213
- [25] J. R. Carlson, H. F. Davis, D. E. Jauch, N. D. Sossong and R. Ellsworth, Measurement of neutral cascade production from negative-kaon-hydrogen at 1.8 gev/c, $K^- p \rightarrow k^0 \Xi^0$, Phys. Rev. D **7**, 2533-2537 (1973) doi:10.1103/PhysRevD.7.2533
- [26] J. Griselin, A. Givernaud, R. Barloutaud, J. Prevost, F. Gandini, C. M. Kiesling, D. E. Plane, W. Wittek, P. Baillon and C. Bricman, *et al.* $K^- p$ Cross-Sections Between 1.1 GeV/c and 1.4 GeV/c, Nucl. Phys. B **93**, 189-216 (1975) doi:10.1016/0550-3213(75)90569-6
- [27] E. Briefel, S. A. Gourevitch, L. Kirsch, P. Schmidt, C. Y. Chang, R. J. Hemingway, B. V. Khoury, A. R. Stottlmyer, G. B. Yodh and R. C. Fernow, *et al.* Search for Ξ^* Production in $K^- p$ Interactions at 2.87 GeV/c, Phys. Rev. D **16**, 2706 (1977) doi:10.1103/PhysRevD.16.2706
- [28] V. Flaminio *et al.* [High-Energy Reactions Analysis Group], COMPILATION OF CROSS-SECTIONS. 2. K^- AND K^+ INDUCED REACTIONS, CERN-HERA-79-02.
- [29] B. K. Agarwal, C. P. Singh, K. J. Narain and A. B. Saxena, $K^- p \rightarrow K^+ \Xi^-$ process in the two-meson-exchange peripheral model, J. Phys. A **4**, L52-L55 (1971) doi:10.1088/0305-

4470/4/3/005

- [30] K. L. Mir and J. K. Storrow, HYPERON EXCHANGE REACTIONS AT HIGH-ENERGIES. 3. BACKWARD $\bar{K}N \rightarrow \Xi K$ SCATTERING, J. Phys. G **8**, 465 (1982) doi:10.1088/0305-4616/8/4/005
- [31] D. A. Sharov, V. L. Korotkikh and D. E. Lanskoy, Phenomenological model for the $\bar{K}N \rightarrow K\Xi$ reaction, Eur. Phys. J. A **47**, 109 (2011) doi:10.1140/epja/i2011-11109-1 [arXiv:1105.0764 [nucl-th]].
- [32] B. C. Jackson, Y. Oh, H. Haberzettl and K. Nakayama, $\bar{K} + N \rightarrow K + \Xi$ reaction and $S = -1$ hyperon resonances, Phys. Rev. C **91**, no.6, 065208 (2015) doi:10.1103/PhysRevC.91.065208 [arXiv:1503.00845 [nucl-th]].
- [33] J. C. David, C. Fayard, G. H. Lamot and B. Saghai, Electromagnetic production of associated strangeness, Phys. Rev. C **53**, 2613-2637 (1996) doi:10.1103/PhysRevC.53.2613